ISSN 1674-1056
http://cpb.iphy.ac.cn
http://iopscience.iop.org/cpb
中国物理 B
Chinese Physics
中国物理 Chinese Physics B

Transport properties of mixing conduction in CaF_2 nanocrystals under high pressure

Ting-Jing Hu(胡廷静), Xiao-Yan Cui(崔晓岩), Jing-Shu Wang(王婧姝), Jun-Kai Zhang(张俊凯), Xue-Fei Li(李雪飞), Jing-Hai Yang(杨景海), Chun-Xiao Gao(高春晓)
Citation: Chin. Phys. B . 2018, 27(1): 016401. **doi:** 10.1088/1674-1056/27/1/016401

Journal homepage: http://cpb.iphy.ac.cn; http://iopscience.iop.org/cpb

What follows is a list of articles you may be interested in

Anomalous behavior and phase transformation of *α* -GaOOH nanocrystals under static compression

Zhao Zhang(张钊), Hang Cui(崔航), Da-Peng Yang(杨大鹏), Jian Zhang(张剑), Shun-Xi Tang(汤顺熙), Si Wu(吴思), Qi-Liang Cui(崔啟良)
Chin. Phys. B . 2017, 26(10): 106402. **doi:** 10.1088/1674-1056/26/10/106402

High pressure electrical transport behavior in SrF_2 nanoplates

Xiao-Yan Cui(崔晓岩), Ting-Jing Hu(胡廷静), Jing-Shu Wang(王婧姝), Jun-Kai Zhang(张俊凯), Xue-Fei Li(李雪飞), Jing-Hai Yang(杨景海), Chun-Xiao Gao(高春晓)
Chin. Phys. B . 2017, 26(4): 046401. **doi:** 10.1088/1674-1056/26/4/046401

Structure phase transformation and equation of state of cerium metal under pressures up to 51 GPa

Ce Ma(马策), Zuo-Yong Dou(窦作勇), Hong-Yang Zhu(祝洪洋), Guang-Yan Fu(付广艳), Xiao Tan(谈笑), Bin Bai(白彬), Peng-Cheng Zhang(张鹏程), Qi-Liang Cui(崔啟良)
Chin. Phys. B . 2016, 25(4): 046401. **doi:** 10.1088/1674-1056/25/4/046401

Carrier behavior of HgTe under high pressure revealed by Hall effect measurement

Hu Ting-Jing, Cui Xiao-Yan, Li Xue-Fei, Wang Jing-Shu, Lü Xiu-Mei, Wang Ling-Sheng, Yang Jing-Hai, Gao Chun-Xiao
Chin. Phys. B . 2015, 24(11): 116401. **doi:** 10.1088/1674-1056/24/11/116401

Structural phase transitions of tellurium nanoplates under pressure

Li Chao, Arfan Bukhtiar, Shen Xi, Kong Pan-Pan, Wang Wei-Peng, Zhao Hao-Fei, Yao Yuan, Zou Bing-Suo, Li Yan-Chun, Li Xiao-Dong, Liu Jing, Jin Chang-Qing, Yu Ri-Cheng
Chin. Phys. B . 2015, 24(3): 036401. **doi:** 10.1088/1674-1056/24/3/036401

Transport properties of mixing conduction in CaF_2 nanocrystals under high pressure*

Ting-Jing Hu(胡廷静)[1], Xiao-Yan Cui(崔晓岩)[1,†], Jing-Shu Wang(王婧姝)[1], Jun-Kai Zhang(张俊凯)[1], Xue-Fei Li(李雪飞)[1], Jing-Hai Yang(杨景海)[1], and Chun-Xiao Gao(高春晓)[2,‡]

[1] *Key Laboratory of Functional Materials Physics and Chemistry of the Ministry of Education, National Demonstration Center for Experimental Physics Education, Jilin Normal University, Siping* 136000, *China*
[2] *State Key Laboratory of Superhard Materials, Jilin University, Changchun* 130012, *China*

(Received 17 August 2017; revised manuscript received 28 September 2017; published online 17 November 2017)

We report on the intriguing electrical transport properties of compressed CaF_2 nanocrystals. The diffusion coefficient, grain and grain boundary resistances vary abnormally at about 14.37 GPa and 20.91 GPa, corresponding to the beginning and completion of the *Fm*3*m*–*Pnma* structural transition. Electron conduction and ion conduction coexist in the transport process and the electron conduction is dominant. The electron transference number of the *Fm*3*m* and *Pnma* phases increases with pressure increasing. As the pressure rises, the F^- ion diffusion and electronic transport processes in the *Fm*3*m* and *Pnma* phases become more difficult. Defects at grains play a dominant role in the electronic transport process.

Keywords: high pressure, electrical properties, phase transitions, transport properties

PACS: 64.60.–i, 72.20.–i, 07.35.+k **DOI:** 10.1088/1674-1056/27/1/016401

1. Introduction

Fluoride materials have been studied for a very long time because they have a wide range of potential optical applications based on their low-energy phonons and high ionicity, which result in less absolute fundamental absorption compared with other oxide or sulfide materials.[1–4] As an important class of fluorides, alkaline earth metal fluorides are dielectric materials, which have been widely used in microelectronic and optoelectronic devices, such as wide-gap insulating overlayers, gate dielectrics, insulators, and buffer layers in semiconductor-on-insulator structures and more advanced three-dimensional (3D) devices.[5–8] As an important type of alkaline earth metal fluoride, calcium fluoride (CaF_2) has become the focus of the semiconductor industry with the development of UV-lithography due to its high transmittance and low absorption coefficient.[9,10] CaF_2 can replace fused silica because it possesses a high laser-induced damage threshold and high transparency until the vacuum ultraviolet region. Therefore, it is considered as the optimal material for deep ultraviolet laser lithography techniques.[11]

With the development of nanometer materials, inorganic nanoscale fluorides are going to play an essential role in various applications based on their unique optical, electrical, and magnetic properties. As a typical anionic conductivity material, the conductive property of CaF_2 is an interesting subject. In 1995, Puin *et al.* measured the conductivity of nanocrystalline CaF_2 and found that the F^- ionic conductivity in nanophase fluorides increases greatly, in contrast to that in the corresponding single crystalline phase.[12] Boulfelfel *et al.* predicted that superionic conduction would emerge in the phase interfaces of the fluorite-to-cotunnite transition of CaF_2.[13] Despite there being many high-pressure studies regarding the phase transitions of CaF_2,[14–17] very few experimental and theoretical works have reported its charge transport behavior under high pressure.

In this work, we conducted a comprehensive investigation on the high-pressure electrical transport properties of CaF_2 nanocrystals by using *in situ* alternate-current (AC) impedance spectra measurements in a diamond anvil cell (DAC) at up to 30.0 GPa. In addition, the variations of diffusion coefficient, bulk and grain boundary resistances with pressure were also discussed.

2. Experimental section

High pressure was conducted by using a Mao–Bell-type diamond anvil cell. The culet of the diamond anvil was 400 μm in diameter. A thin film of metal molybdenum was deposited on to the DAC surface and the microcircuit on the surface was utilized in the measurements of resistivity under high pressure. The fabrication process of the microcircuit on diamond anvils has been reported in the previous paper.[18–20] The completed microcircuit and the profile of our designed

*Project supported by the National Natural Science Foundation of China (Grant Nos. 11374131, 11674404, 11404137, and 61378085), Program for the Development of Science and Technology of Jilin Province, China (Grant Nos. 201201079 and 20150204085GX), Twentieth Five-Year Program for Science and Technology of Education Department of Jilin Province, China (Grant No. 20150221), and Open Project of State Key Laboratory of Superhard Materials (Jilin University), China (Grant No. 201710).

†Corresponding author. E-mail: xycuimail@163.com
‡Corresponding author. E-mail: cc060109@qq.com

© 2018 Chinese Physical Society and IOP Publishing Ltd

DAC are shown in Fig. 1.

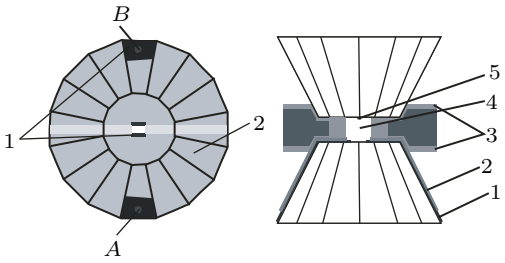


Fig. 1. (a) Completed microcircuit on diamond anvil and (b) the profile of our designed DAC. 1 is Mo, 2 is an alumina layer, 3 is an insulating layer, 4 is the sample chamber, and 5 is ruby. *A* and *B* are the contact ends of the microcircuit.

A T301 stainless steel was used as a gasket that was pre-indented into 60 μm in thickness. Using a laser drilling machine, a hole was drilled at the center of the indentation with 250 μm in diameter. To insure that sample and gasket, electrodes and gasket are insulated to each other, an insulating layer that mixed cubic boron nitride powder and epoxy was compressed into the indentation. Subsequently, a sample chamber of 150 μm was drilled by using a laser drilling machine. The pressure was calibrated by the R1 fluorescence peak of ruby. Ruby's R1 fluorescence peak was detected by a Renishaw in Via Raman spectrometer. To avoid additional error on the electrical transport measurements, no pressure-transmitting medium was used. By using a Solartron 1260 impedance analyzer equipped with Solartron 1296 dielectric interface, the impedance spectroscopy was measured. A voltage signal with amplitude of 1 V and frequency ranged from 0.1 Hz to 10^7 Hz was applied to the sample. The CaF_2 nanocrystals were prepared using a liquid-solid-solution (LSS) solvothermal route, and the sample is square shaped with a mean size of length around 8±2 nm.[21]

3. Results and discussion

Figure 2 illustrates the Z''–Z' plots of the impedance spectra. The X-axis is the real part of impedance (Z'), and the Y-axis is the imaginary part of impedance (Z'').

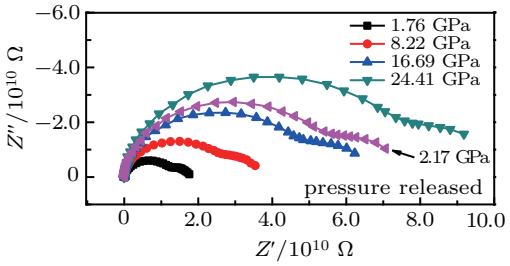


Fig. 2. (color online) The Z''–Z' plots of impedance spectra.

To deeply analyze the impedance spectroscopy, the obtained data are usually modeled by an equivalent circuit. The ionic conduction of F^- can be revealed by the Z'–$\omega^{-1/2}$ plots of the impedance spectra. Figure 3 shows the Z'–$\omega^{-1/2}$ plots of CaF_2 nanocrystals.

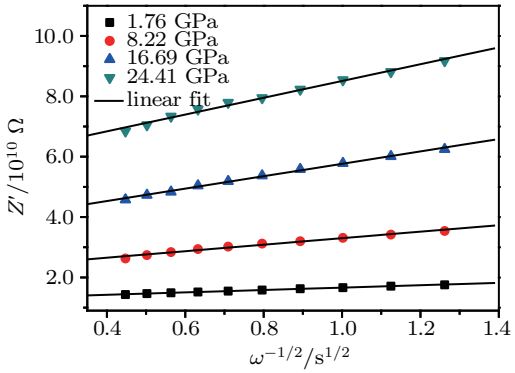


Fig. 3. (color online) The Z'–$\omega^{-1/2}$ plots of CaF_2 nanocrystals at low frequency.

From Fig. 3, it can be seen that Z' and $\omega^{-1/2}$ are linear in the low frequency region, which indicates the existence of F^- ions diffusion at low frequency. Thus, to describe the F^- ions diffusion, a Warburg impedance element was added to the equivalent circuit. If the charge carriers are only F^- ions, the Z''–Z' plot in the low frequency region would be a line with 45° to the X axis such as the hollow circle plot in Fig. 4.

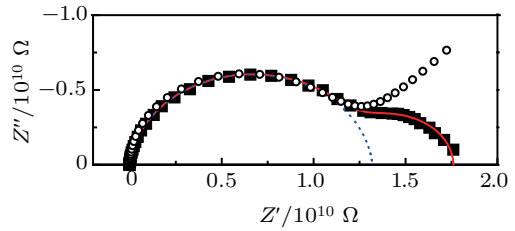


Fig. 4. (color online) The Z''–Z' plot of impedance spectra at 1.76 GPa. The solid square is the experimental result. The hollow circle is the result with only F^- ions conduction. The continuous line is the simulated spectrum. R_1 and R_2 are the intercepts of the Nyquist plot on the X axis.

Thus, electron conduction and ion conduction coexist in the transport process of CaF_2 nanocrystals. We used the equivalent circuit in Fig. 5 to analyze the conduction mechanism of CaF_2 nanocrystals under high pressure.

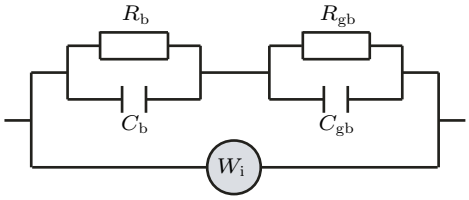


Fig. 5. The equivalent circuit model for mixing conduction of electron and ion. R_b is the grain resistance, R_{gb} is the grain boundary resistance, C_b is the grain capacitance, C_{gb} is the grain boundary capacitance, and W_i is the Warburg impedance.

From Fig. 4, it can be seen that the simulated spectrum well agrees with the experimental data, indicating that the

equivalent circuit model we used is reasonable. It can also indicate the validity of considering that the charge carriers in CaF_2 nanocrystals include both ions and electrons.

Because F^- ions and electrons coexist in CaF_2 nanocrystals, it is necessary to distinguish each carrier contribution to the transport process. The transference number[22] is usually used to describe the contribution of each type of carrier to the transport process. The F^- ion transference number (t_i) can be expressed as

$$t_i = (R_2 - R_1)/R_2,$$

and the electron transference number (t_e) can be expressed as

$$t_e = R_1/R_2,$$

where R_1 and R_2 are the intercepts of the Nyquist plot on the X axis (Fig. 4). Figure 6 shows the variation of ion and electron transference numbers with pressure. It can be seen that the transference numbers of ion and electron change discontinuously at about 14.37 GPa and 20.91 GPa. According to our previous XRD results,[21] under compression the *Pnma* structure appears in the $Fm3m$ phase at about 14.0 GPa. However, the transition is rather sluggish, and both the low-pressure and *Pnma* phases co-exist up to a pressure of 22.2 GPa.[21] Therefore, the discontinuous changes of ion and electron transference numbers should be caused by the $Fm3m$–*Pnma* phase transition of CaF_2 nanocrystals under high pressure. In the whole pressure region, the electron conduction has the dominant contribution to the transport process of CaF_2 nanocrystals, and the electron transference number of the $Fm3m$ and *Pnma* phases increases as the pressure rises.

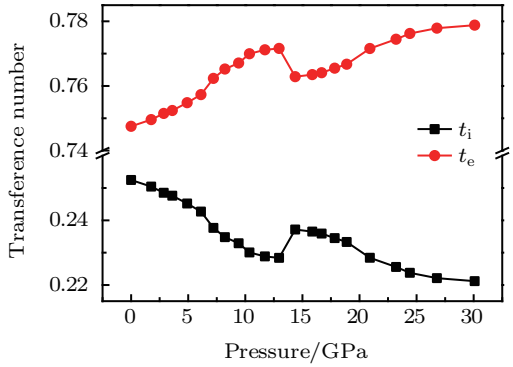


Fig. 6. (color online) The variation of ion and electron transference numbers with pressure.

Due to the existence of the ionic conduction, in the low frequency region Z' and $\omega^{-1/2}$ can be expressed as

$$Z' = Z'_0 + \sigma\omega^{-1/2},$$

where is a constant, and σ is the Warburg coefficient. By linearly fitting the Z'–$\omega^{-1/2}$ curves, the Warburg coefficient under high pressure was obtained.

The ion diffusion coefficient can be expressed as

$$D_i = 0.5\left(\frac{RT}{AF^2\sigma C}\right)^2,$$

where R is the ideal gas constant , T is the temperature, $F$is the Faraday constant, and C is the molar concentration. We set the F^- ion diffusion coefficient at 0 GPa as D_0, the values of D_i/D_0 under different pressures were obtained and shown in Fig. 7(a).

Using the equivalent circuit model (Fig. 5), the impedance spectra were fitted by the Zview2 impedance analysis software, and the grain resistance (R_b) and grain boundary resistance (R_{gb}) under various pressures were obtained and shown in Fig. 7.

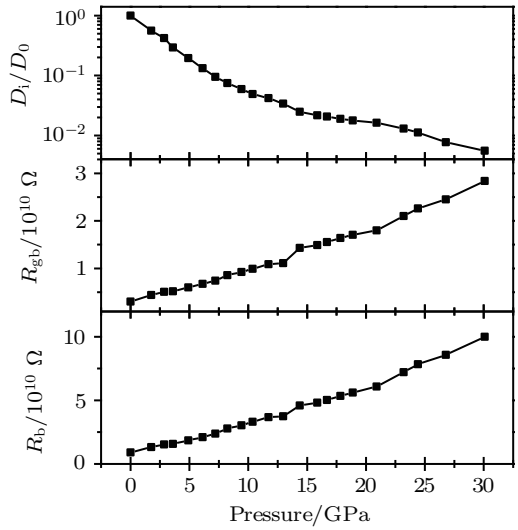


Fig. 7. The pressure dependence of (a) diffusion coefficient, (b) grain resistance, and (c) grain boundary resistance of CaF_2 nanocrystals. D_0 is the diffusion coefficient at 0 GPa.

From Fig. 7, it can be seen that the diffusion coefficient, grain and grain boundary resistances vary abnormally at about 14.37 GPa and 20.91 GPa, corresponding to the beginning and completing of the $Fm3m$–*Pnma* structural transition.[21] These results indicate that the electrical transport behavior has detectable changes as the phase transition occurs.

In the $Fm3m$ and *Pnma* phases, the diffusion coefficient of the F^- ion decreases, whereas the grain resistance and the grain boundary resistance increase as the pressure rises; which indicates that both the F^- ions diffusion and electronic transport become more difficult under compression. In the whole pressure range, the grain resistance is larger than the grain boundary resistance, which indicates that the grain resistance has a major contribution to the total resistance and defects at grains play a dominant role in the electronic transport process.

4. Conclusions

The electrical transport properties of CaF_2 nanocrystals have been investigated by *in situ* impedance measurement up

to 30 GPa. Each parameter changes discontinuously at about 14.37 GPa and 20.91 GPa, corresponding to the beginning and completing of CaF_2 nanocrystals phase transition under high pressure. Electron conduction and ion conduction coexist in the transport process and the electron conduction is dominant. The electron transference number of the *Fm*3*m* and *Pnma* phases increases with pressure increasing. As the pressure rises, the F^- ion diffusion and electronic transport processes in the *Fm*3*m* and *Pnma* phases become more difficult. Defects at grains play a dominant role in the electronic transport process.

References

[1] Justel T, Nikol H and Ronda C 1998 *Angew. Chem. Int. Edn.* **37** 3085
[2] Feldmann C, Roming M and Trampert K 2006 *Small* **2** 1248
[3] Quan Z W, Yang D M, Yang P P, Zhang X M, Lian H Z, Liu X M and Lin J 2008 *Inorg. Chem.* **47** 9509.
[4] Gao P, Xie Y and Li Z 2006 *Eur. J. Inorg. Chem.* **16** 3261
[5] Mao Y B, Zhang F and Wong S S 2006 *Adv. Mater.* **18** 1895
[6] Wang W S, Zhen L, Xu CY, Chen J Z and Shao W Z 2009 *Appl. Mater. Interfaces* **1** 780
[7] Singh R, Sinha S, Chou P, Hsu N J and Radpour F 1989 *J. Appl. Phys.* **66** 6179
[8] Quan Z W, Yang D M, Li C X, Yang P P, Cheng Z Y, Yang J, Kong D Y and Lin J 2009 *Mater. Res. Bull.* **44** 1009
[9] Dong Y J, Zhou G Q, Yang W Q, Su L B and Xu J 2004 *J. Inorg. Mater.* **19** 449
[10] Westerhoff T, Knapp K and Moersen E 1998 *Proc. SPIE* **3424** 10
[11] Liberman V, Bloomstein T M, Rothschild M, Sedlacek J H C, Uttaro R S, Bates A K, Peski C V and Orvek K 1999 *J. Vac. Sci. Technol. B* **17** 3273
[12] Puin W and Heitjans P 1995 *Nanostruct. Mater.* **6** 885
[13] Boulfelfel SE, Zahn D, Hochrein O, Grin Y and Leoni S 2006 *Phys. Rev. B* **74** 094106
[14] Dorfman S M, Jiang F, Mao Z, Kubo A, Meng Y, Prakapenka V B and Duffy T S 2010 *Phys. Rev. B* **81** 174121
[15] Morris E, Groy T and Leinenweber K 2001 *J. Phys. Chem. Solids* **62** 1117
[16] Kavner A 2008 *Phys. Rev. B* **77** 224102
[17] Wu X, Qin S and Wu Z Y 2006 *Phys. Rev. B* **73** 134103
[18] Cui X Y, Hu T J, Han Y H, Gao C X, Peng G, Liu C L, Wu B J, Wang Y, Liu B, Ren W B, Li Y, Su N N, Zou G T, Du F and Chen G 2010 *Chin. Phys. Lett.* **27** 036402
[19] Hu T J, Cui X Y, Li X F, Wang J S, Yang J H and Gao C X 2015 *Chin. Phys. Lett.* **32** 016402
[20] Hu T J, Cui X Y, Li X F, Wang J S, Lv X M, Wang L S, Yang J H and Gao C X 2015 *Chin. Phys. B* **24** 116401
[21] Wang J S, Hao J, Wang Q S, Jin Y X, Li F F, Liu B, Li Q J, Liu B B and Cui Q L 2011 *Phys. Status Solidi B* **248** 1115
[22] Wang Q L, Liu C L, Gao Y, Ma Y Z, Han Y H and Gao C X 2015 *Appl. Phys. Lett.* **106** 132902